# Diagnostic value of computed high b-value whole-body diffusion-weighted imaging for primary prostate cancer

Arita, Yuki; Yoshida, Soichiro; Waseda, Yuma; Takahara, Taro; Ishii, Chikako; Ueda, Ryo; Kwee, Thomas C.; Miyahira, Kei; Ishii, Ryota; Okuda, Shigeo

*Published in:*
European Journal of Radiology

*DOI:*
10.1016/j.ejrad.2021.109581



*Publication date:*
2021

European Journal of Radiology 137 (2021) 109581

Contents lists available at ScienceDirect

European Journal of Radiology

journal homepage: www.elsevier.com/locate/ejrad

# Diagnostic value of computed high b-value whole-body diffusion-weighted imaging for primary prostate cancer

Yuki Arita [a,b,*], Soichiro Yoshida [b,c], Yuma Waseda [c], Taro Takahara [b,d], Chikako Ishii [b], Ryo Ueda [e], Thomas C. Kwee [f], Kei Miyahira [a], Ryota Ishii [g], Shigeo Okuda [a], Masahiro Jinzaki [a], Yasuhisa Fujii [c]

[a] Department of Radiology, Keio University School of Medicine, 35, Shinanomachi, Shinjuku-ku, Tokyo, 160-8582, Japan
[b] Department of Radiology, Advanced Imaging Center Yaesu Clinic, 2-1-18, Nihonbashi, Chuo-ku, Tokyo, 103-0027, Japan
[c] Department of Urology, Tokyo Medical and Dental University Graduate School, 1-5-45, Yushima, Bunkyo-ku, Tokyo, 113-8519, Japan
[d] Department of Biomedical Engineering, Tokai University School of Engineering, 143, Shimokasuya, Isehara, Kanagawa, 259-1193, Japan
[e] Office of Radiation Technology, Keio University Hospital, 35, Shinanomachi, Shinjuku-ku, Tokyo, 160-8582, Japan
[f] Department of Radiology, Nuclear Medicine, and Molecular Imaging, University Medical Center Groningen, Hanzeplein 1, P.O. Box 30.001, 9700 RB, Groningen, the Netherlands
[g] Biostatistics Unit, Clinical and Translational Research Center, Keio University Hospital, 35, Shinanomachi, Shinjuku-ku, Tokyo, 160-8582, Japan

ARTICLE INFO

*Keywords:*
Prostate cancer
Magnetic resonance imaging
Diffusion-weighted magnetic resonance imaging
Whole-body imaging

ABSTRACT

*Purpose:* To investigate the utility of post-acquisition computed diffusion-weighted imaging (cDWI) for primary prostate cancer (PCa) evaluation in biparametric whole-body MRI (bpWB-MRI).

*Methods:* Patients who underwent pelvic MRI for PCa screening and subsequent bpWB-MRI for staging were included.

Two radiologists assessed the diagnostic performance of the following datasets for clinically significant PCa diagnosis (grade group ≥2 according to the Prostate Imaging-Reporting and Data System, version 2.1): $bpMRI_{2000}$ (axial DWI scans with a b-value of 2,000 s/mm$^2$ + axial T2WI scans from pre-biopsy pelvic MRI), computed $bpWB\text{-}MRI_{2000}$ (computed WB-DWI scans with a b-value of 2,000 s/mm$^2$ + axial WB-T2WI scans), and native $bpWB\text{-}MRI_{1000}$ (native axial WB-DWI scans with a b-value of 1,000 s/mm$^2$ + axial WB-T2WI scans). Systemic biopsy was used as reference standard.

*Results:* Fifty-one patients with PCa were included. The areas under the curve (AUCs) of $bpMRI_{2000}$ (0.89 for reader 1 and 0.86 for reader 2) and computed $bpWB\text{-}MRI_{2000}$ (0.86 for reader 1 and 0.83 for reader 2) were significantly higher ($p < 0.001$) than those of native $bpWB\text{-}MRI_{1000}$ (0.67 for both readers). No significant difference was observed between the AUCs of $bpMRI_{2000}$ and computed $bpWB\text{-}MRI_{2000}$ ($p = 0.10$ for reader 1 and $p = 0.25$ for reader 2).

*Conclusions:* The diagnostic performance of computed $bpWB\text{-}MRI_{2000}$ was similar to that of dedicated pelvic $bpMRI_{2000}$ for primary PCa evaluation. cDWI can be recommended for implementation in standard WB-MRI protocols to facilitate a one-step evaluation for concurrent detection of primary and metastatic PCa.

*Abbreviations:* PSA, prostate-specific antigen; bpWB-MRI, biparametric whole-body magnetic resonance imaging; STIR, short inversion time inversion recovery; T2WI, T2-weighted imaging; PI-RADS, Prostate Imaging and Reporting and Data System; PZ, peripheral zone; TZ, transitional zone; DWI, diffusion-weighted imaging; AUC, area under the curve; mpMRI, multiparametric magnetic resonance imaging; DWIBS, diffusion-weighted whole-body imaging with background body signal suppression; PET, positron emission tomography; TR, repetition time; TE, echo time; ADC, apparent diffusion coefficient; TI, inversion time; $bpMRI_{2000}$, axial DWI with a b-value of 2,000 s/mm$^2$ + axial T2WI from pre-biopsy pelvic MRI; native $bpWB\text{-}MRI_{1000}$, native axial WB-DWI with a b-value of 1,000 s/mm$^2$ (native $WB\text{-}DWI_{1000}$) + axial WB-T2WI; computed $bpWB\text{-}MRI_{2000}$, computed WB-DWI with a b-value of 2,000 s/mm$^2$ + axial WB-T2WI; $pDWI_{2000}$, axial DWI with a b-value of 2,000 s/mm$^2$; native $WB\text{-}DWI_{1000}$, native axial WB-DWI with a b-value of 1,000 s/mm$^2$; computed $WB\text{-}DWI_{2000}$, computed WB-DWI with a b-value of 2,000 s/mm$^2$; ROC, receiver operating characteristic.

* Corresponding author at: Department of Radiology, Keio University School of Medicine, Tokyo, Japan.
*E-mail addresses:* yarita@rad.med.keio.ac.jp (Y. Arita), s-yoshida.uro@tmd.ac.jp (S. Yoshida), yuma_waseda@tmhp.jp (Y. Waseda), tarorin@gmail.com (T. Takahara), ishii.chikako@nifty.com (C. Ishii), dyeorua@gmail.com (R. Ueda), thomaskwee@gmail.com (T.C. Kwee), kmiyahira@rad.med.keio.ac.jp (K. Miyahira), rishii@keio.jp (R. Ishii), okuda@rad.med.keio.ac.jp (S. Okuda), jinzaki@rad.med.keio.ac.jp (M. Jinzaki), y-fujii.uro@tmd.ac.jp (Y. Fujii).

https://doi.org/10.1016/j.ejrad.2021.109581
Received 8 November 2020; Received in revised form 26 January 2021; Accepted 1 February 2021
Available online 6 February 2021

## 1. Introduction

Locoregional therapy for metastatic prostate cancer has recently garnered considerable interest [1–4], as randomized clinical trials have demonstrated the benefit of prostate-directed radiotherapy in patients with oligometastatic disease and metastasis-directed therapy in patients with oligorecurrent prostate cancer [5,6]. Robust imaging techniques that can detect active disease in the metastatic lesions and at the primary prostate cancer site are essential for the application of this lesion-targeted approach.

Magnetic resonance imaging (MRI) is being increasingly used for prostate cancer evaluation, particularly in the screening for clinically significant cancer [7,8]. Diffusion-weighted imaging (DWI) is deemed an essential functional sequence of multiparametric MRI (mpMRI) of the prostate and is acknowledged as such in the Prostate Imaging and Reporting and Data System (PI-RADS) [9,10]. Advances in MR devices and the concept of whole-body (WB) DWI with background body signal suppression (DWIBS) have made it possible to perform WB-MRI with DWI (i.e., WB-DWI) in a single examination. WB-DWI has excellent clinical potential, with widespread use as a staging tool for osseous and soft-tissue metastases in advanced prostate cancer [11]. Furthermore, the European Organization for Research and Treatment of Cancer has positioned WB-DWI as the potential first choice for monitoring and evaluating the treatment response of bone metastases, along with $^{18}$F-fluorocholine and $^{11}$C-choline positron emission tomography (PET) [12].

Given the excellent diagnostic performance of DWI with high b-value of 2,000 s/mm$^2$ for primary prostate cancer, the employment of high b-value would facilitate the use of WB-DWI as a one-step examination for primary and metastatic prostate cancer. However, owing to the restricted scanning time, a standard WB-DWI protocol usually employs relatively low b-values of 0 and 1,000 s/mm$^2$ in clinical settings, which may be suboptimal for primary prostate cancer evaluation.

Computed DWI is a computational technique that synthesizes DW images at any arbitrary (high) b-value from a DWI dataset that has been obtained with at least two different (lower) b-values [13], which permits the acquisition of a DW image with a high b-value from standard WB-DW images. Blackledge et al. applied this post-processing technique to WB-DWI, which resulted in improvement in the detection accuracy for systemic metastatic lesions in patients with prostate cancer. Applying the computed DWI technique to a WB-DWI protocol would be beneficial if the computed high b-value DW image would be sufficient for evaluation of the local prostate cancer in the pelvis without the need for additional pelvic mpMRI, because computed DWI requires no additional acquisition time and can be generated automatically by the MRI software after image acquisition.

In this study, we investigated the feasibility of post-acquisition management using the computed DWI technique for the use of biparametric WB-MRI (bpWB-MRI) as a one-step examination for primary and metastatic prostate cancer. We analyzed the diagnostic value of computed WB-DW images with a b-value of 2,000 s/mm$^2$ for primary prostate cancer.

## 2. Patients and methods

The study protocol was approved by the medical ethics committee of our institution (approval number: M2018-069), and the need for written informed consent was waived owing to the retrospective nature of the study.

### 2.1. Patients

Among patients suspected to have prostate cancer who underwent pelvic MRI for prostate cancer screening, including T2-weighted imaging (T2WI) and DWI, prior to saturation prostate biopsy, 56 patients who subsequently underwent WB-MRI for metastatic prostate cancer staging were included in this study. Patients who had received prior treatment (n = 3) or whose DWI data quality was degraded due to susceptibility artifacts (n = 2) were excluded, and the remaining 51 patients were included in the analysis (Fig. 1).

### 2.2. Image acquisition: pelvic MRI protocol

Pelvic MRI was performed using a 1.5-T system (Intera Achieva 1.5-T; Philips Healthcare, Best, the Netherlands). The parameters for DWI were as follows: repetition time (TR)/echo time (TE) of 5,000/80 ms; and three different b-values (0, 1,000, and 2,000 s/mm$^2$). Apparent diffusion coefficient (ADC) maps were generated from the native DWI dataset. The following parameters were used for T2WI: TR/TE, 2,000/151 ms.

### 2.3. Image acquisition: WB-MRI protocol

WB-MRI was performed from the skull base to the mid-thighs with a 1.5- or 3.0-T system (Intera Achieva 1.5-T/Ingenia 3.0-T; Philips Healthcare). The parameters for DWIBS were as follows: TR/TE/inversion time (TI) of 7,457/70/180 ms (1.5-T system), and 5,300/69/250 ms (3.0-T system); with b-values of 0 and 1,000 s/mm$^2$; and a total of three stations [14]. ADC maps were generated from the native DWIBS dataset. The following parameters were used for T2WI: TR/TE of 3,000/90 ms (1.5-T system), and 1,231/85 ms (3.0-T system). The pelvic station of the acquired DWIBS and T2WI included the volume from at least the level of L1 to the proximal femurs. The sequence parameters used for pelvic MRI and WB-MRI at 1.5- and 3.0-T are shown in Supplementary Table 1.

### 2.4. Generation of computed high b-value DW images from the pelvic station of WB-DW images

Computed DW images with a b-value of 2,000 s/mm$^2$ were generated from the native DWIBS dataset based on standard monoexponential model fitting using medical image processing software (OsiriX v. 6.5.1; Pixmeo, Geneva, Switzerland) (Fig. 2).

### 2.5. Image analysis

#### 2.5.1. Subjective image quality assessment

Three bpMRI datasets were sent to our institutional imaging server system for review:

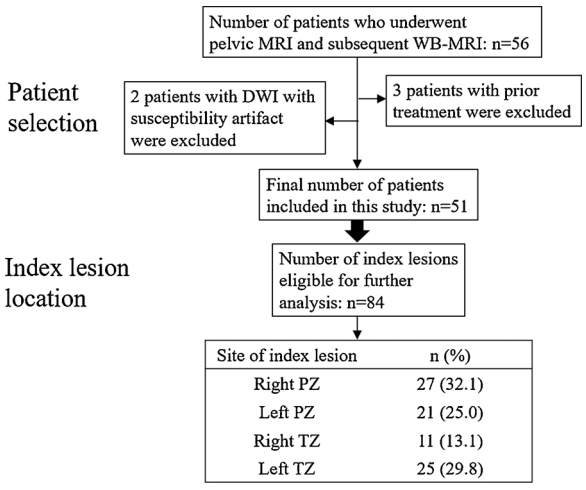


**Fig. 1. Flowchart of patient selection.**
MRI, magnetic resonance imaging; WB-MRI, whole-body MRI; DWI, diffusion-weighted imaging; PZ, peripheral zone; TZ, transitional zone.

(a) $bpMRI_{2000}$; axial DWI scans with a b-value of 2,000 s/mm$^2$ ($pDWI_{2000}$) + axial T2WI scans from pre-biopsy pelvic MRI,
(b) computed $bpWB\text{-}MRI_{2000}$; computed WB-DWI scans with a b-value of 2,000 s/mm$^2$ (computed $WB\text{-}DWI_{2000}$) + axial WB-T2WI scans, and
(c) native $bpWB\text{-}MRI_{1000}$; native axial WB-DWI scans with a b-value of 1,000 s/mm$^2$ (native $WB\text{-}DWI_{1000}$) + axial WB-T2WI scans

All three bpMRI datasets were reviewed along with the ADC maps for reference, using a multimodality workstation (SDS viewer; TechMatrix Corporation, Tokyo, Japan). The type of sequence and parameters were anonymized prior to reading on the workstation. The three bpMRI datasets were evaluated independently by two board-certified uroradiologists with 37 and 7 years of experience, who were blinded to all clinical and pathological data, including the previous imaging data and findings. The three bpMRI datasets of each patient were assigned anonymous identifiers and reviewed in a random order.

While reviewing each DWI scan ($pDWI_{2000}$, native $WB\text{-}DWI_{1000}$, and computed $WB\text{-}DWI_{2000}$), readers 1 and 2 subjectively evaluated each image on a scale of 1–5 (with a score of 1 corresponding to the worst quality and a score of 5 corresponding to the highest quality) for the following items: suppression of a normal-appearing prostate, absence of image distortion of the prostate, and overall image quality (the image quality was evaluated per DW-series) [15,16].

### 2.5.2. PI-RADS scoring evaluation

For each of the four prostate regions i.e., right and left transitional zone (TZ), and right and left peripheral zone (PZ), DWI and T2WI scans of each bpMRI dataset were scored using a five-point scoring system, with DWI as the dominant sequence for the PZ and T2WI for the TZ, in order to obtain an overall score, according to the PI-RADS v2.1 criteria [10]. A PI-RADS score between 1 and 5 was assigned, where 1 denoted a low likelihood and 5 indicated a high likelihood of clinically significant prostate cancer (grade group ≥2 tumors) [10]. The tumor with the highest score (index lesion) was used to calculate the score for that prostate region in patients with multiple tumors in one prostate region.

### 2.5.3. Reference standard

The results of systemic biopsy with/without targeted prostate biopsy were used as the reference standard for the presence or absence of prostate cancer in each of the four prostate regions [17]. The pathologically dominant lesion was defined as the one with the highest-grade group or the largest size (in case of equal grade grouping) for each side in the PZ and TZ. Grade groups were assigned according to the 2014 International Society of Urological Pathology consensus conference guidelines. Grade group ≥2 tumors were considered as clinically significant prostate cancer.

### 2.5.4. Statistical analysis

Exact Wilcoxon signed-rank tests were used to compare the three different DWI scans with respect to the readers' assessment. Receiver operating characteristic (ROC) curve analysis based on logistic regression was performed to assess the diagnostic performance of the three bpMRI datasets for prostate cancer on a region basis. The areas under the curve (AUCs) were compared using a two-variable chi-squared test. The sensitivity and specificity of any two pairs of the three bpMRI datasets for prostate cancer on a region basis (with a cutoff PI-RADS score of ≥3) were compared using the McNemar test. Interobserver agreement was assessed with a consistency test and by calculating the weighted kappa coefficients. All $p$-values were two-sided and $p$-values $< 0.05$ were

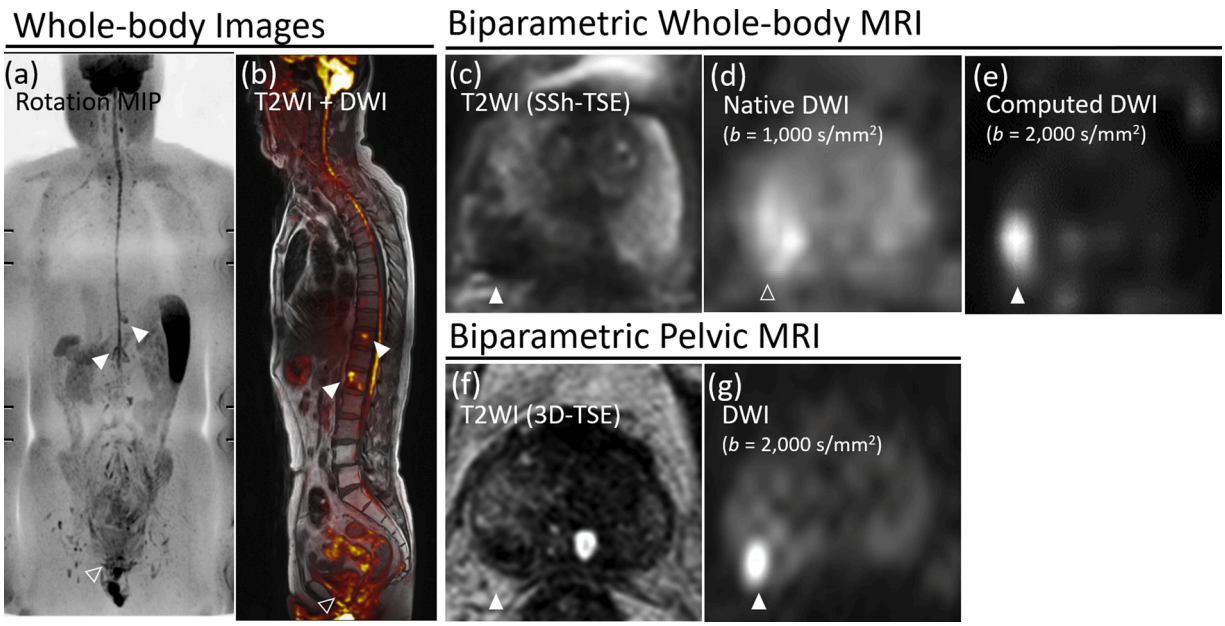


**Fig. 2. Representative images of a 71-year-old man with a 10-mm adenocarcinoma in the right prostate lobe peripheral zone (cT2aN0M1b, grade group 4, PSA 30.6 ng/mL).**
(**a**) Maximum intensity projection of native DWI at a b-value of 1,000 s/mm$^2$ from WB-MRI and (**b**) sagittal fusion image of T2WI + native DWI at a b-value of 1,000 s/mm$^2$ from WB-MRI show an abnormally high-signal intensity focus on the eleventh thoracic vertebra, and the first lumbar vertebra (arrowheads), corresponding to vertebral metastases, but fail to demonstrate the primary prostate cancer focus (non-specifically increased signal intensity on DWI); (**c**) Axial native DWI scan with a b-value of 1,000 s/mm$^2$ from WB-MRI with ambiguously increased signal intensity; (**d**) Axial T2WI scan from WB-MRI (single-shot turbo spin-echo sequence was used) and (**f**) T2WI scan from conventional pelvic MRI showing a low-signal intensity focus within normal-appearing prostate tissue in the right peripheral zone (arrowheads); (**e**) Axial computed DWI scan with a b-value of 2,000 s/mm$^2$ from WB-MRI and (**g**) native DWI scan with a b-value of 2,000 s/mm$^2$ from conventional pelvic MRI displaying a high-signal intensity focus corresponding to the location of an abnormal signal on the T2WI scan (arrowheads), corresponding to a PI-RADS score of 4.
Abbreviations: PSA, prostate-specific antigen; MRI, magnetic resonance imaging; WB-MRI, whole-body MRI; MIP, maximum intensity projection; DWI, diffusion-weighted imaging; T2WI, T2-weighted imaging; SSh-TSE, single-shot turbo spin-echo; 3D-TSE, three-dimensional TSE; PI-RADS, Prostate Imaging and Reporting and Data System.

considered statistically significant. ROC curve analysis was performed using IBM SPSS Statistics v20 (IBM Corp., Armonk, NY, USA) and the R-package pROC, v1.15.3 (R Foundation for Statistical Computing, Vienna, Austria). Other statistical analyses were performed using SAS software v9.0 (SAS Institute, Cary, NC, USA).

## 3. Results

### 3.1. Characteristics of the patients and prostate cancer lesions

The clinicopathological data are shown in Table 1. The median time intervals from prostate biopsy and pelvic MRI to WB-MRI were 4 weeks (range 1–6 weeks) and 6 weeks (range 2–8 weeks), respectively. The 51 patients included in this study harbored a total of 84 index lesions: grade group 1 (n = 7), grade group 2 (n = 20), grade group 3 (n = 17), grade group 4 (n = 19), and grade group 5 (n = 21).

### 3.2. Comparison of subjective DW image quality

The subjective image quality grading of each DWI dataset is shown in Table 2. Suppression of the normal-appearing prostate tissue signal, absence of image distortion, and overall image quality were better for the $pDWI_{2000}$ and computed $WB\text{-}DWI_{2000}$ images than for native $WB\text{-}DWI_{1000}$ images ($p < 0.05$ for both readers). No significant difference was found in the other comparisons of the DWI datasets. A representative case of subjective quality of distortion is shown in Supplementary Fig. 1.

### 3.3. Comparison of the three bpMRI datasets for primary prostate cancer detection using PI-RADS

The diagnostic performance of the three bpMRI datasets was compared using PI-RADS v2.1. The weighted kappa coefficients between reader 1 and reader 2 were 0.84 (95 % CI 0.80–0.91), 0.82 (95 % CI 0.76–0.88), and 0.76 (95 % CI 0.65–0.82) for $bpMRI_{2000}$, computed $bpWB\text{-}MRI_{2000}$, and native $bpWB\text{-}MRI_{1000}$, respectively. The AUCs of the three datasets for diagnosing clinically significant prostate cancer are shown in Fig. 3, with $bpMRI_{2000}$ and computed $WB\text{-}MRI_{2000}$ providing better diagnostic performance than native $WB\text{-}MRI_{1000}$ ($p < 0.05$ for both readers). No significant difference was found between $bpMRI_{2000}$ and computed $bpWB\text{-}MRI_{2000}$ ($p = 0.10$, 0.25, for reader 1 and reader 2, respectively). The sensitivity/specificity values (%) for all prostate cancer lesions and clinically significant prostate cancer lesions (grade group ≥2 tumors) with a cutoff PI-RADS score of ≥3 are shown in Table 3. No significant difference was found between $bpMRI_{2000}$ and computed $bpWB\text{-}MRI_{2000}$ for all prostate cancer lesions and clinically significant prostate cancer lesions for both readers. No significant difference in the diagnostic performance was found between 1.5- and 3.0-T settings, as shown in Supplementary Table 2.

**Table 1**
Characteristics of the patients (n = 51) and their prostate cancer lesions (n = 84).

| Variables | |
|---|---|
| Patient characteristics | |
| Age, years | 69 (58–84) [a] |
| PSA level, ng/mL | 14.8 (4.1–248.5) [a] |
| ALP level, IU/L | 219 (132–368) [a] |
| MR setting | |
| 1.5/3.0-T | 33 (64.7) / 18 (35.3) [b] |
| Prostate cancer characteristics | |
| Clinical stage | |
| T1c/T2a/T2b/T2c/T3a/T3b | 8 (15.7) / 15 (29.4) / 8 (15.7) / 7 (13.7) / 8 (15.7) / 5 (9.8) [b] |
| Site of the index lesion | |
| Rt. PZ/Lt. PZ/Rt. TZ/Lt. TZ | 27 (32.1) / 21 (25.0) /11 (13.1) / 25 (29.8) [b] |
| Maximum cancer length, mm | 7.4 (0–23.0) [a] |
| Gleason score of the dominant lesion | |
| 6 | 7 (8.4) [b] |
| 7 | 37 (44.0) [b] |
| 8–10 | 40 (47.6) [b] |

PSA: prostate-specific antigen, ALP: alkaline phosphatase, Rt: right, Lt: left, PZ: peripheral zone, TZ: transitional zone.
Data are presented as [a] median (range) or [b] n (%).

**Table 2**
Comparison of the subjective quality of DWI.

| Parameter | Reader | $pDWI_{2000}$ (A) | computed $WB\text{-}DWI_{2000}$ (B) | native $WB\text{-}DWI_{1000}$ (C) | *p*-value (A vs. B) |
|---|---|---|---|---|---|
| Suppression of normal-appearing prostate in the PZ | 1 | 4.5 | 4.4 | 3.5 | 0.18 |
| | 2 | 4.4 | 4.5 | 3.6 | 0.42 |
| Absence of image distortion | 1 | 3.9 | 3.7 | 3.1 | 0.09 |
| | 2 | 4.0 | 3.8 | 3.0 | 0.20 |
| Overall image quality | 1 | 4.3 | 4.1 | 3.3 | 0.10 |
| | 2 | 4.2 | 4.0 | 3.4 | 0.09 |

DWI: diffusion-weighted imaging, $pDWI_{2000}$: pelvic DWI with a b-value of 2,000 s/mm$^2$, Computed $WB\text{-}DWI_{2000}$: computed DWI with a b-value of 2,000 s/mm$^2$ from whole-body DWI, Native $WB\text{-}DWI_{1000}$: DWI with a b-value of 1,000 s/mm$^2$ from whole-body DWI, PZ: peripheral zone. Note: A score of 1 corresponds to the worst quality and a score of 5 corresponds to the highest quality. *$p < 0.05$, statistically significant.

## 4. Discussion

We investigated the feasibility of using computed high b-value WB-DWI for primary prostate cancer evaluation. Our study demonstrated that the diagnostic performance of computed $bpWB\text{-}DWI_{2000}$ was comparable to that of dedicated pelvic bpMRI for primary prostate cancer evaluation. It should also be noted that the diagnostic performance values that were demonstrated in the present study (AUCs of $bpWB\text{-}MRI_{2000}$ and pelvic $bpMRI_{2000}$ of 0.83–0.89) approach the results of a recent meta-analysis on the diagnostic accuracy of pelvic bpMRI for prostate cancer (AUC of 0.90) [18]. Based on these results, post-acquisition management using the computed DWI technique makes bpWB-MRI a potential robust one-step imaging analysis modality for detecting active disease at the primary tumor site in the prostate and at metastatic sites throughout the body.

The interreader agreement of the three bpMRI datasets in this study was good to excellent, which is in line with a recent report by Brembilla et al. [19]. In the image quality analysis, all the subjective quality measures analyzed (background suppression, absence of image distortion, and overall image quality) received significantly better scores on computed $WB\text{-}DWI_{2000}$ images than on native $WB\text{-}DWI_{1000}$ images. The better image quality of computed $WB\text{-}DWI_{2000}$ translated into improved diagnostic performance, as both readers achieved significantly better AUCs than those with native $WB\text{-}DWI_{1000}$ for local prostate cancer detection. On the other hand, no significant difference was found between $pDWI_{2000}$ and computed $WB\text{-}DWI_{2000}$ with respect to image quality and diagnostic performance (i.e. AUCs, sensitivity values, and specificity values). Based on the results, no significant difference in the diagnostic performance was found between 1.5- and 3.0-T settings, which is consistent with the results of a recent meta-analysis by Woo, et al. [20], though the patient cohort in the current study was relatively small.

The computed DWI technique, which is a post-acquisition procedure, requires no additional image acquisition time [13,21], and pelvic bpMRI and computed $bpWB\text{-}MRI_{2000}$ have been shown to provide comparable diagnostic performance. Therefore, incorporating computed high b-value DWI into standard clinical WB-MRI protocols for patients with prostate cancer may overcome the shortcomings of WB-DWI (i.e.

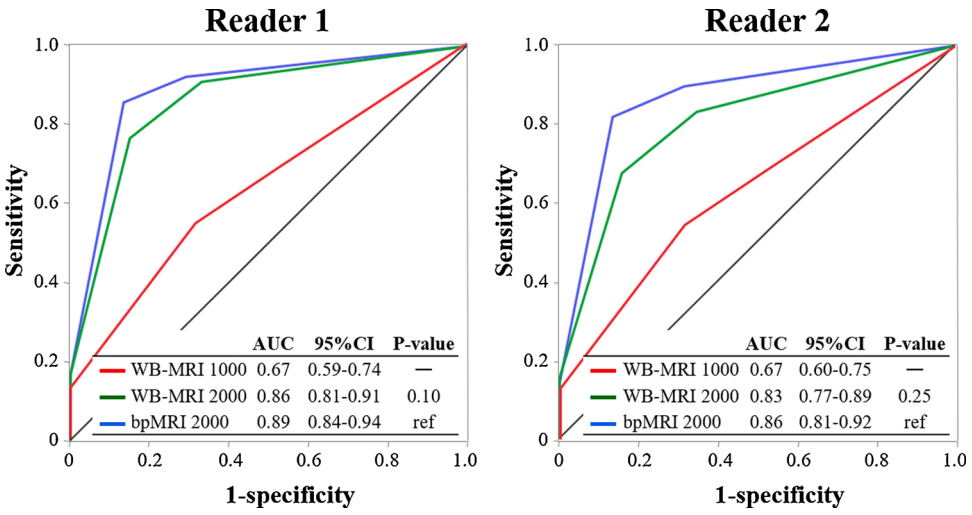


**Fig. 3. Receiver operating characteristic curves of the three biparametric MRI datasets.**
The AUCs of $bpMRI_{2000}$ and computed bpWB-$MRI_{2000}$ were significantly higher than those of native bpWB-$MRI_{1000}$ ($p < 0.001$, for both readers), while there was no significant difference between $bpMRI_{2000}$ and computed bpWB-$MRI_{2000}$ ($p = 0.10$, 0.25, for reader 1 and reader 2, respectively).
Abbreviations: AUC, area under the curve; CI, confidence interval; bpMRI, biparametric magnetic resonance imaging; WB, whole-body; DWI, diffusion-weighted imaging; T2WI, T2-weighted imaging; $bpMRI_{2000}$, axial DWI with a b-value of 2,000 s/mm$^2$ ($pDWI_{2000}$) + axial T2WI from pre-biopsy pelvic MRI; computed bpWB-$MRI_{2000}$, computed WB-DWI with a b-value of 2,000 s/mm$^2$ (computed WB-$DWI_{2000}$) + axial WB-T2WI; native bpWB-$MRI_{1000}$, native axial WB-DWI with a b-value of 1,000 s/mm$^2$ (native WB-$DWI_{1000}$) + axial WB-T2WI.

**Table 3**
Comparison of the diagnostic performance of the three datasets of biparametric MRI for primary prostate cancer using a cutoff score of ≥3 in the PI-RADS version 2.1.

| Parameter | Reader | Biparametric MRI datasets | | | |
|---|---|---|---|---|---|
| | | $bpMRI_{2000}$ (A) | computed bpWB-$MRI_{2000}$ (B) | native bpWB-$MRI_{1000}$ (C) | *p*-value (A vs B) |
| Sensitivity (all tumors) | 1 | 86.9 % | 84.5 % | 65.5 % | 0.32 |
| | 2 | 84.5 % | 81.0 % | 65.5 % | 0.37 |
| Specificity (all tumors) | 1 | 70.8 % | 65.8 % | 47.5 % | 0.11 |
| | 2 | 67.5 % | 64.2 % | 50.8 % | 0.48 |
| Sensitivity (Grade group ≥2 tumors) | 1 | 92.2 % | 90.9 % | 68.8 % | 0.56 |
| | 2 | 89.6 % | 87.0 % | 68.8 % | 0.53 |
| Specificity (Grade group ≥2 tumors) | 1 | 70.9 % | 66.9 % | 48.8 % | 0.20 |
| | 2 | 67.7 % | 65.4 % | 52.0 % | 0.60 |

MRI: magnetic resonance imaging, PI-RADS: Prostate Imaging and Reporting and Data System, DWI: diffusion-weighted imaging, T2WI: T2-weighted imaging, $bpMRI_{2000}$: axial DWI with b-value of 2,000 s/mm$^2$ + axial T2WI from pre-biopsy pelvic MRI, computed bpWB-$MRI_{2000}$: computed WB-DWI with b-value of 2,000 s/mm$^2$ + axial WB-T2WI, native bpWB-$MRI_{1000}$: native axial WB-DWI with b-value of 1,000 s/mm$^2$ + axial WB-T2WI.
*$p < 0.05$, statistically significant.

relatively low b-values of 0 and 1,000 s/mm$^2$ in clinical settings) for primary prostate cancer evaluation [13]. Furthermore, WB-MRI is relatively low cost and does not involve any radiation exposure, which renders it more amenable for frequent follow-up imaging. According to previous reports, computed high b-value prostate DWI showed better diagnostic performance for prostate cancer evaluation than native prostate DWI with a b-value of 1,000 s/mm$^2$ [15,22]. In our study, we applied the computed DWI technique to WB-MRI and reconfirmed the usefulness of computed high b-value DWI for prostate cancer diagnosis.

In patients with treatment failure after local definitive therapy (radical prostatectomy or primary radiotherapy), elevation in prostate-specific antigen levels precedes the detection of recurrent lesions. It is necessary to determine the site of recurrent lesions (local or distant), and the number of metastatic lesions in such patients, in order to optimize salvage treatment, depending on the risk of subsequent metastases and mortality [23]. Once local recurrence is confirmed by prostate biopsy, salvage radical prostatectomy, cryoablation, brachytherapy, and high-intensity focused ultrasound can be used for treating biochemical recurrence after radiation therapy. Therefore, computed high b-value WB-DWI, which enables the detection of active disease at the primary tumor site in the prostate and at metastatic sites throughout the body, can be a useful adjunct for patients after local therapy.

Our study has several limitations. First, we divided the prostate into four regions, and only the index lesion with the highest pathological grade group or size was analyzed in patients with multiple lesions, which might have resulted in selection bias. Nevertheless, the concept of the index lesion has been widely used in previous studies, including studies on PI-RADS [7,10,24–26]. Second, bpWB-MRI was performed after prostate biopsy, which might have affected the image quality, although the median time interval between prostate biopsy and bpWB-MRI was 4 weeks. Third, the results of systemic biopsy with/-without targeted prostate biopsy were used as the reference standard, since radical prostatectomy is uncommon in this patient population. Fourth, the pelvic DWI sequence (b-values of 0, 1000 and 2000) does not comply with standards as suggested in PI-RADS. Finally, this retrospective single-center study included a relatively small sample size. Further larger, multicenter validation studies are necessary to confirm the results of this study.

## 5. Conclusion

The diagnostic performance of computed high-b value bpWB-MRI is comparable to that of dedicated pelvic bpMRI for detecting primary prostate cancer. Application of the computed DWI technique to standard WB-MRI protocols may facilitate one-step examination for concurrent detection of primary and metastatic prostate cancer.

## Funding

This research did not receive any specific grant from funding agencies in the public, commercial, or not-for-profit sectors.

## CRediT authorship contribution statement

**Yuki Arita:** Investigation, Writing - original draft. **Soichiro Yoshida:** Writing - review & editing, Visualization. **Yuma Waseda:** Resources, Visualization. **Taro Takahara:** Resources, Data curation. **Chikako Ishii:** Resources, Data curation. **Ryo Ueda:** Resources, Data curation. **Thomas C. Kwee:** Writing - review & editing. **Kei Miyahira:**

Resources, Data curation. **Ryota Ishii:** Resources, Data curation. **Shigeo Okuda:** Resources, Data curation. **Masahiro Jinzaki:** Writing - review & editing. **Yasuhisa Fujii:** Supervision, Project administration.

## Declaration of Competing Interest

The authors declare that the research was conducted in the absence of any commercial or financial relationships that could be construed as a potential conflict of interest.

## Acknowledgments

The authors thank Mr. Mizuki Akatsuka and Mr. Atsushi Tachibana for their help with data collection.

## Appendix A. Supplementary data

Supplementary material related to this article can be found, in the online version, at doi:https://doi.org/10.1016/j.ejrad.2021.109581.

## References

[1] S.R. Leyh-Bannurah, S. Gazdovich, L. Budäus, et al., Local therapy improves survival in metastatic prostate cancer, Eur. Urol. 72 (2017) 118–124, https://doi.org/10.1016/j.eururo.2017.03.020.
[2] P. Ost, B.A. Jereczek-Fossa, N. Van As, et al., Progression-free survival following stereotactic body radiotherapy for oligometastatic prostate cancer treatment-naive recurrence: a multi-institutional analysis, Eur. Urol. 69 (2016) 9–12, https://doi.org/10.1016/j.eururo.2015.07.004.
[3] S. Yoshida, T. Takahara, Y. Arita, et al., Progressive site-directed therapy for castration-resistant prostate cancer: localization of the progressive site as a prognostic factor, Int. J. Radiat. Oncol. Biol. Phys. 105 (2019) 376–381, https://doi.org/10.1016/j.ijrobp.2019.06.011.
[4] D. Tilki, R.S. Pompe, M. Bandini, et al., Local treatment for metastatic prostate cancer: a systematic review, Int. J. Urol. 25 (2018) 390–403, https://doi.org/10.1111/iju.13535.
[5] C.C. Parker, N.D. James, C.D. Brawley, et al., Radiotherapy to the primary tumour for newly diagnosed, metastatic prostate cancer (STAMPEDE): a randomized controlled phase 3 trial, Lancet 392 (2018) 2353–2366, https://doi.org/10.1016/S0140-6736(18)32486-3.
[6] P. Ost, D. Reynders, K. Decaestecker, et al., Surveillance or metastasis-directed therapy for oligometastatic prostate cancer recurrence: a prospective, randomized, multicenter phase II trial, J. Clin. Oncol. 36 (2018) 446–453, https://doi.org/10.1200/JCO.2017.75.4853.
[7] S. Verma, P.L. Choyke, S.C. Eberhardt, et al., The current state of MR imaging-targeted biopsy techniques for detection of prostate cancer, Radiology 285 (2017) 343–356, https://doi.org/10.1148/radiol.2017161684.
[8] A.B. Rosenkrantz, S. Verma, P. Choyke, et al., Prostate magnetic resonance imaging and magnetic resonance imaging targeted biopsy in patients with a prior negative biopsy: a consensus statement by AUA and SAR, J. Urol. 196 (2016) 1613–1618, https://doi.org/10.1016/j.juro.2016.06.079.
[9] J.C. Weinreb, J.O. Barentsz, P.L. Choyke, et al., PI-RADS prostate imaging – reporting and data system: 2015, version 2, Eur. Urol. 69 (2016) 16–40, https://doi.org/10.1016/j.eururo.2015.08.052.
[10] B. Turkbey, A.B. Rosenkrantz, M.A. Haider, et al., Prostate imaging reporting and data system version 2.1: 2019 update of prostate imaging reporting and data system version 2, Eur. Urol. 76 (2019) 340–351, https://doi.org/10.1016/j.eururo.2019.02.033.
[11] F.E. Lecouvet, J. El Mouedden, L. Collette, et al., Can whole-body magnetic resonance imaging with diffusion-weighted imaging replace Tc 99m bone scanning and computed tomography for single-step detection of metastases in patients with high-risk prostate cancer? Eur. Urol. 62 (2012) 68–75, https://doi.org/10.1016/j.eururo.2012.02.020.
[12] F.E. Lecouvet, J.N. Talbot, C. Messiou, et al., Monitoring the response of bone metastases to treatment with magnetic resonance imaging and nuclear medicine techniques: a review and position statement by the European Organization for Research and Treatment of Cancer imaging group, Eur. J. Cancer 50 (2014) 2519–2531, https://doi.org/10.1016/j.ejca.2014.07.002.
[13] M.D. Blackledge, M.O. Leach, D.J. Collins, et al., Computed diffusion-weighted MR imaging may improve tumor detection, Radiology 261 (2011) 573–581, https://doi.org/10.1148/radiol.11101919.
[14] T. Takahara, Y. Imai, T. Yamashita, et al., Diffusion-weighted whole-body imaging with background body signal suppression (DWIBS): technical improvement using free breathing, STIR and high resolution 3D display, Radiat. Med. 22 (2004) 275–282. PMID: 15468951.
[15] A.B. Rosenkrantz, H. Chandarana, N. Hindman, et al., Computed diffusion-weighted imaging of the prostate at 3T: impact on image quality and tumour detection, Eur. Radiol. 23 (2013) 3170–3177, https://doi.org/10.1007/s00330-013-2917-8.
[16] A.B. Rosenkrantz, H. Chandarana, J. Pfeuffer, et al., Zoomed echo-planar imaging using parallel transmission: impact on image quality of diffusion-weighted imaging of the prostate at 3T, Abdom. Imaging 40 (2015) 120–126, https://doi.org/10.1007/s00261-014-0181-2.
[17] A. Matoso, J.I. Epstein, Defining clinically significant prostate cancer on the basis of pathological findings, Histopathology 74 (2019) 135–145, https://doi.org/10.1111/his.13712.
[18] S. Woo, C.H. Suh, S.Y. Kim, J.Y. Cho, S.H. Kim, M.H. Moonet, Head-to-head comparison between biparametric and multiparametric MRI for the diagnosis of prostate cancer: a systematic review and meta-analysis, Am. J. Roentgenol. 211 (2018) W226–W241, https://doi.org/10.2214/AJR.18.19880.
[19] G. Brembilla, P. Dell'Oglio, A. Stabile, et al., Interreader variability in prostate MRI reporting using Prostate Imaging Reporting and Data System version 2.1, Eur. Radiol. 30 (2020) 3383–3392, https://doi.org/10.1007/s00330-019-06654-2.
[20] S. Woo, C.H. Suh, S.Y. Kim, J.Y. Cho, S.H. Kim, Diagnostic performance of prostate imaging reporting and data system version 2 for detection of prostate cancer: a systematic review and diagnostic meta-analysis, Eur. Urol. 72 (2017) 177–188, https://doi.org/10.1016/j.eururo.2017.01.042.
[21] G. Gandaglia, P.I. Karakiewicz, A. Briganti, et al., Impact of the site of metastases on survival in patients with metastatic prostate cancer, Eur. Urol. 68 (2015) 325–334, https://doi.org/10.1016/j.eururo.2014.07.020.
[22] Y. Ueno, S. Takahashi, K. Kitajima, T. Kimura, I. Aoki, F. Kawakami, H. Miyake, Y. Ohno, K. Sugimura, Computed diffusion-weighted imaging using 3-T magnetic resonance imaging for prostate cancer diagnosis, Eur. Radiol. 12 (2013) 3509–3516, https://doi.org/10.1007/s00330-013-2958-z.
[23] D. Tilki, F. Preisser, M. Graefen, et al., External validation of the European Association of Urology biochemical recurrence risk groups to predict metastasis and mortality after radical prostatectomy in a European cohort, Eur. Urol. 75 (2019) 896–900, https://doi.org/10.1016/j.eururo.2019.03.016.
[24] H.U. Ahmed, The index lesion and the origin of prostate cancer, N. Engl. J. Med. 361 (2009) 1704–1706, https://doi.org/10.1056/NEJMcibr0905562.
[25] S.R.J. Bott, H.U. Ahmed, R.G. Hindley, et al., The index lesion and focal therapy: an analysis of the pathological characteristics of prostate cancer, BJU Int. 106 (2010) 1607–1611, https://doi.org/10.1111/j.1464-410X.2010.09436.x.
[26] M. Karavitakis, M. Winkler, P. Abel, et al., Histological characteristics of the index lesion in whole-mount radical prostatectomy specimens: implications for focal therapy, Prostate Cancer Prostatic Dis. 14 (2011) 46–52, https://doi.org/10.1038/pcan.2010.16.